第 49 卷 第 4 期/2022 年 2 月/中国激光 研究论文

中国激光

双 Sagnac 环滤波器的传输特性分析和实验研究

崔文翔[1]，周雪芳[1*]，胡淼[1]，毕美华[1]，杨国伟[1]，李齐良[1]，王天枢[2]

[1]杭州电子科技大学通信工程学院，浙江 杭州 310018；

[2]长春理工大学空间光电技术研究所，吉林 长春 130022

摘要 利用传输矩阵理论，对一种双 Sagnac 环滤波器的传输特性进行了理论推导和仿真分析，该滤波器由两段不同长度的保偏光纤(PMF)并联构成。仿真结果表明：该滤波器具有偏振无关和通道间隔可调的特性。对双 Saganc 环滤波器的传输谱进行了实验测试，通过调节滤波器中的偏振控制器(PC)，可以实现通道间隔的可调操作，调整入射光的偏振态并不会改变光谱形状，与理论分析得到的结论一致。最后，为了验证双 Saganc 环滤波器在激光器系统中的通道间隔可调特性，设计了一种基于四波混频(FWM)效应和双 Sagnac 环滤波器的通道间隔可调多波长掺铒光纤激光器。实验结果表明：该激光器可以输出通道间隔为 0.9 nm 或 0.35 nm 的多波长激光，这与仿真结果以及测量结果一致。

关键词 光纤光学；光滤波器；传输矩阵理论；双 Sagnac 环；通道间隔可调；偏振无关

中图分类号 O436 **文献标志码** A **doi**：10.3788/CJL202249.0406006

1 引 言

光纤 Sagnac 环具有成本低廉、损耗低和结构简单等优良特性，因此常常被用于制作光纤传感器和光纤 Sagnac 干涉仪滤波器[1-4]。近年来，光纤 Sagnac 环或者改进型光纤 Sagnac 环被许多学者用来作为多波长光纤激光器的滤波器[5-9]。Kim 等[5]提出了一种基于高双折射 Sagnac 环梳状滤波器的多波长掺铒光纤激光器，但是输出的多波长并不是很稳定。这是因为掺铒光纤在室温下具有均匀展宽的特性，所以激光器无法实现稳定的多波长输出[10]。为了实现稳定的多波长输出，就需要引入抑制模式竞争的机制。Chen 等[6]提出了一种基于光子晶体光纤 Sagnac 环梳状滤波器的多波长掺铒光纤激光器，其中具有高双折射率和高非线性的光子晶体光纤 Sagnac 环既能作为梳状滤波器，也能产生四波混频(FWM)效应抑制模式竞争，从而获得稳定的多波长输出。Wang 等[7]提出了一种基于非线性环形镜(Nonlinear Optical Loop Mirror，NOLM)和 Sagnac 环梳状滤波器的多波长掺铒光纤激光器，其中高双折射的 Saganc 环用于产生多波长激光，NOLM 用于抑制模式竞争。Cheng 等[8]提出了一种基于啁啾布拉格光栅和 Sagnac 环梳状滤波器的可切换四波长掺铒光纤激光器，其中高双折射的 Saganc 环用于产生多波长输出，偏振烧孔(Polarization Hole Burning，PHB)效应用于提高输出激光的稳定性以及实现多波长激光的切换。

上述激光器都是基于单个 Sagnac 环梳状滤波器的多波长掺铒光纤激光器，其主要缺陷是滤波器的通道间隔无法改变。He 等[11]设计了一种基于双 Sagnac 环滤波器的多波长掺铒光纤激光器，双 Sagnac 环滤波器由两段不同长度的保偏光纤(PMF)组成，通过调节偏振控制器(PC)，可以实现最多四波长的输出，但是由于缺乏抑制模式竞争的器件，四波长输出非常不稳定。朱可等[12]设计了一种基于双 Sagnac 环滤波器的多波长掺铒光纤激光器，双 Sagnac 环滤波器由一段 PMF 和一段少模光纤组成，通过改变腔内的偏振态产生 PHB 效应，从而实现稳定的三波长输出，最多有六波长输出。但

收稿日期：2021-06-09；**修回日期**：2021-07-09；**录用日期**：2021-07-26

基金项目：国家自然科学基金(61705055)、浙江省重点研发计划项目(2019C01G1121168)、浙江省科技厅公益基础项目(LGG19F050001)

通信作者：*zhouxf@hdu.edu.cn

是研究者没有对这种双 Sagnac 环滤波器的传输特性进行仿真模拟。Tang 等[13]设计了一种基于双 Sagnac 环滤波器的多波长掺铒光纤激光器，实现了稳定的五波长激光输出，输出波长最大数目为六，输出激光的模式均为 LP_{11} 模。但是在对这种双 Sagnac 环滤波器的滤波特性进行理论分析时，只考虑了入射光是线偏振光的情况。虽然在双 Sagnac 环滤波器的仿真和测量中证明了双 Sagnac 环滤波器通道间隔的可变性，但是在激光器的实验中只观察到了一种通道间隔，研究者认为强烈的模式竞争导致激光器无法在更小的通道间隔下实现多波长激光的输出。上述基于双 Sagnac 环滤波器的理论研究和实验探究仍存在一些不足，限制了双 Sagnac 环滤波器在多波长光纤激光器和光纤传感技术等领域中的应用。

针对上述双 Sagnac 环滤波器特性理论研究的不足，本文对双 Sagnac 环滤波器的特性进行了理论推导和仿真分析，并对其传输特性进行了实验测试。测试结果证明了滤波器的偏振无关和通道间隔可调的特性。设计了一种基于 FWM 效应和双 Sagnac 环滤波器的多波长掺铒光纤激光器，实现了通道间隔可调谐的多波长激光，实验结果与仿真结果吻合。本文的研究结果为双 Sagnac 环滤波器在光纤激光器和光纤传感技术中的应用提供了理论支撑和实验参考。

2　基本原理和实验仿真

双 Sagnac 环滤波器的原理图如图 1 所示。该滤波器由三个耦合器(OC)、两个 PC 和两段不同长度的 PMF 组成。入射光从端口 1 进入 OC 1 后被分为两束光，一束光经过端口 3 沿顺时针方向传输，然后分别通过 PC 和 PMF，到达 OC 1 的端口 4，另一束光经过端口 4 沿逆时针方向传输，然后分别通过 PMF 和 PC，到达 OC 1 的端口 3，最后两束光在 OC 1 的端口 2 相干输出。

根据耦合模理论，OC 的传输矩阵可以表示为

$$\boldsymbol{T}_{\mathrm{OC}}=\begin{pmatrix}\sqrt{1-k}\,\boldsymbol{I} & \mathrm{i}\sqrt{k}\,\boldsymbol{I}\\ \mathrm{i}\sqrt{k}\,\boldsymbol{I} & \sqrt{1-k}\,\boldsymbol{I}\end{pmatrix},\tag{1}$$

式中：$\boldsymbol{I}$ 表示单位矩阵；k 为 OC 的耦合比。OC 1 的端口 3、OC 2 的端口 2 和 OC 3 的端口 2 为 OC 的直通端，OC 1 的端口 4、OC 2 的端口 3 和 OC 3 的端口 3 为 OC 的耦合端。

当光入射 PC 时，光的偏振方向会旋转 θ 角度，因此 PC 的琼斯矩阵可以表示为

$$\boldsymbol{J}_{\mathrm{PC}}(\theta)=\begin{pmatrix}\cos\theta & \sin\theta\\ -\sin\theta & \cos\theta\end{pmatrix},\tag{2}$$

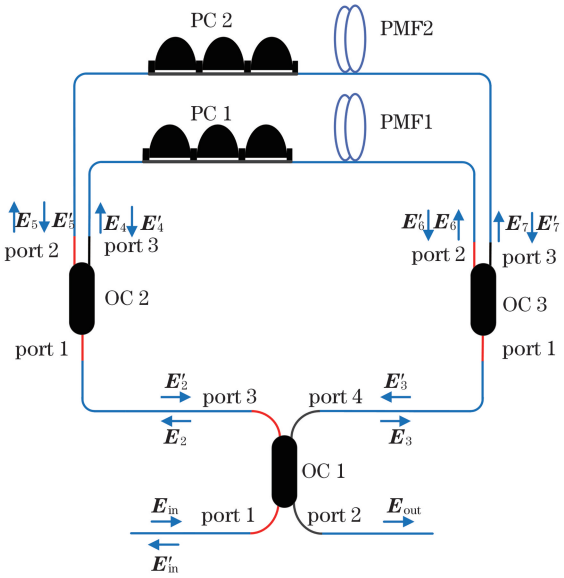

图 1　双 Sagnac 环滤波器的原理图

Fig. 1　Principle diagram of double Sagnac loop

反向传输的光经过偏振控制器的琼斯矩阵为 $\boldsymbol{J}_{\mathrm{PC}}^{-1}(\theta)=\boldsymbol{J}_{\mathrm{PC}}(-\theta)$。

当光经过 PMF 时，PMF 的琼斯矩阵可以表示为

$$\boldsymbol{J}_{\mathrm{PMF}}=\begin{pmatrix}\mathrm{e}^{-\mathrm{i}\varphi} & 0\\ 0 & \mathrm{e}^{\mathrm{i}\varphi}\end{pmatrix},\tag{3}$$

式中：$\varphi=\pi\Delta nL_{\mathrm{PMF}}/\lambda$，其中 L_{PMF} 是 PMF 的长度，Δn 是 PMF 快慢轴的有效双折射率之差，λ 是光的波长。反向传输的光经过偏振控制器的琼斯矩阵为 $\boldsymbol{J}_{\mathrm{PMF}}^{-1}=\boldsymbol{J}_{\mathrm{PMF}}$。

假定入射光的光场矢量为

$$\boldsymbol{E}_{\mathrm{in}}=\begin{pmatrix}E_x\\ E_y\end{pmatrix},\tag{4}$$

式中：E_x 和 E_y 分别表示输入光场矢量在 x、y 坐标轴上的投影。

当光进入 OC 1 时，有

$$\begin{pmatrix}\boldsymbol{E}_3\\ \boldsymbol{E}_2\end{pmatrix}=\boldsymbol{T}_{\mathrm{OC\,1}}\begin{pmatrix}\boldsymbol{E}_{\mathrm{in}}\\ \boldsymbol{0}\end{pmatrix},\tag{5}$$

式中：$\boldsymbol{E}_2$ 为经过 OC 1 端口 3 后的光场矢量；$\boldsymbol{E}_3$ 为经过 OC 1 端口 4 后的光场矢量。

在顺时针方向上，有

$$\begin{pmatrix}\boldsymbol{E}_6'\\ \boldsymbol{E}_7'\end{pmatrix}=\begin{pmatrix}\boldsymbol{J}_{\mathrm{PMF\,1}}\cdot\boldsymbol{J}_{\mathrm{PC\,1}}(\theta_1) & \boldsymbol{0}\\ \boldsymbol{0} & \boldsymbol{J}_{\mathrm{PMF\,2}}\cdot\boldsymbol{J}_{\mathrm{PC\,2}}(\theta_2)\end{pmatrix}\times\boldsymbol{T}_{\mathrm{OC\,2}}\begin{pmatrix}\boldsymbol{E}_2\\ \boldsymbol{0}\end{pmatrix},\tag{6}$$

式中：$\boldsymbol{E}_6'$ 为顺时针传输光经过 PC 1 后又经过 PMF 1 的光场矢量；$\boldsymbol{E}_7'$ 为顺时针传输光经过 PC 2 后又经过 PMF 2 的光场矢量；θ_1 为顺时针传输光经过 PC

1 后改变的偏转角度；θ_2 为顺时针传输光经过 PC 2 后改变的偏转角度。

返回 OC 1 的 4 端口的电场强度为

$$\boldsymbol{E}'_3=\mathrm{i}\sqrt{k_3}\cdot\boldsymbol{E}'_6+\sqrt{1-k_3}\cdot\boldsymbol{E}'_7,\tag{7}$$

式中：k_3 为 OC 3 的耦合比。

在逆时针方向上，有

$$\begin{pmatrix}\boldsymbol{E}'_5\\ \boldsymbol{E}'_4\end{pmatrix}=\begin{pmatrix}\boldsymbol{J}_{\mathrm{PC\,2}}(-\theta_2)\cdot\boldsymbol{J}_{\mathrm{PMF\,2}} & \boldsymbol{0}\\ \boldsymbol{0} & \boldsymbol{J}_{\mathrm{PC\,1}}(-\theta_1)\cdot\boldsymbol{J}_{\mathrm{PMF\,1}}\end{pmatrix}\times\boldsymbol{T}_{\mathrm{OC\,3}}\begin{pmatrix}\boldsymbol{E}_3\\ \boldsymbol{0}\end{pmatrix},\tag{8}$$

式中：$\boldsymbol{E}'_4$ 为逆时针传输光经过 PMF 1 后又经过 PC 1 后的光场矢量；$\boldsymbol{E}'_5$ 为逆时针传输光经过 PMF 2 后又经过 PC 2 后的光场矢量。

返回 OC 1 端口 3 的光场矢量为

$$\boldsymbol{E}'_2=\mathrm{i}\sqrt{k_2}\cdot\boldsymbol{E}'_5+\sqrt{1-k_2}\cdot\boldsymbol{E}'_4,\tag{9}$$

式中：k_2 为 OC 2 的耦合比。

最后两束光回到 OC 1，有

$$\begin{pmatrix}\boldsymbol{E}'_{\mathrm{in}}\\ \boldsymbol{E}_{\mathrm{out}}\end{pmatrix}=\boldsymbol{T}_{\mathrm{OC\,1}}\begin{pmatrix}\boldsymbol{E}'_3\\ \boldsymbol{E}'_2\end{pmatrix},\tag{10}$$

式中：$\boldsymbol{E}'_{\mathrm{in}}$ 为滤波器的反射光场矢量；$\boldsymbol{E}_{\mathrm{out}}$ 为滤波器的透射光场矢量。

当 OC 1 的耦合比 $k_1=k_2=k_3=0.5$ 时，透射谱的传输函数为

$$T=\frac{|\boldsymbol{E}_{\mathrm{out}}|^2}{|\boldsymbol{E}_{\mathrm{in}}|^2}=\frac{1}{4}(\sin\theta_1\cos\varphi_1+\sin\theta_2\cos\varphi_2)^2,\tag{11}$$

式中：φ_1 为光经过 PMF1 的快轴和慢轴之后产生的相位差；φ_2 为光经过 PMF 2 的快轴和慢轴之后产生的相位差。

从透射谱的传输函数可以看出，该滤波器是偏振无关的。在仿真实验中，将 PMF 1 和 PMF 2 的长度分别设置为 6.6 m 和 13.51 m，$\Delta n_{\mathrm{PMF\,1}}=4.0\times10^{-4}$，$\Delta n_{\mathrm{PMF\,2}}=5.1\times10^{-4}$。通过适当设置 PC 1 和 PC 2 的偏转角度，可以调控滤波器的通道间隔。当设置 $\theta_1=\pi/6$，$\theta_2=0$ 时，仿真的透射谱如图 2(a)所示，通道间隔为 $\Delta\lambda_1=\lambda^2/(\Delta n_{\mathrm{PMF\,1}}\times L_{\mathrm{PMF\,1}})=0.9$ nm。当设置 $\theta_1=0$，$\theta_2=\pi/6$ 时，仿真的透射谱如图 2(b)所示，通道间隔为 $\Delta\lambda_2=\lambda^2/(\Delta n_{\mathrm{PMF\,2}}\times L_{\mathrm{PMF\,2}})=0.35$ nm。

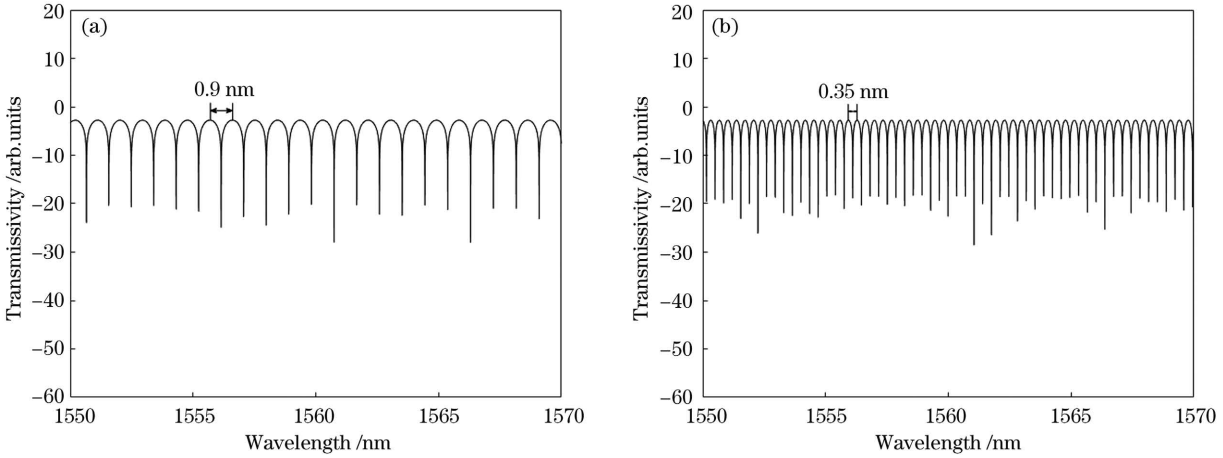

图 2　不同条件下双 Sagnac 环滤波器的仿真透射谱。(a)$\theta_1=\pi/6$，$\theta_2=0$；(b)$\theta_1=0$，$\theta_2=\pi/6$

Fig. 2　Simulated transmission spectra of double Sagnac loop filter under different conditions. (a) $\theta_1=\pi/6$, $\theta_2=0$; (b) $\theta_1=0$, $\theta_2=\pi/6$

3　分析与讨论

3.1　基于两段 PMF 的双 Sagnac 环滤波器的传输特性测量

为了证明理论分析和仿真结果的正确性，搭建了用于测试双 Sagnac 环滤波器传输特性的实验装置，如图 3 所示。在该实验装置中，掺铒光纤放大器(Erbium Doped Fiber Amplifier，EDFA)为输入光源，偏振无关隔离器(Polarization Independent Isolator，PI-ISO)用于保证光单向振荡，PC-1 用于调节入射光的偏振态。在双 Sagnac 环滤波器中，三个耦合器的耦合比均为 0.5，两段 PMF 的长度分别为 6.6 m 和 13.51 m，其中 $\Delta n_{\mathrm{PMF\,1}}=4.0\times10^{-4}$，$\Delta n_{\mathrm{PMF\,2}}=5.1\times10^{-4}$。端口 2 的输出光谱和 EDFA 的输出光谱由分辨率为 0.02 nm 的光谱分析仪(Optical Spectrum Analyzer，OSA)测量。而双 Sagnac 环滤波器的传输谱可以由端口 2 的输出光谱减去 EDFA 的输出光谱得到。通过仔细调节双 Saganc 环滤波器中 PC 1 和 PC 2 的偏转角度，可以得到三种不同状态的传输光谱，如图 4 所示。从

图 4(a)可以看出，光谱的通道间隔为 0.9 nm，对应于图 2(a)的仿真结果。从图 4(b)可以看出，光谱的通道间隔为 0.35 nm，对应于图 2(b)的仿真结果。图 4(c)对应于(11)式中 θ_1 和 θ_2 均不为 0 的情况，可以看出，此时的光谱处于无规律的状态，这与两段式 Lyot-Sagnac 环滤波器的透射光谱特性类似[14-15]。当光谱的通道间隔为 0.9 nm 且保持 PC 1 和 PC 2 的状态不变时，调节 PC-1，从图 5(a)中可以看出，光谱形状保持不变。当光谱的通道间隔为 0.35 nm 且不改变双 Sagnac 环滤波器中的 PC 状态时，任意调节 PC-1 的偏转角度，从图 5(b)中可以看出，光谱形状同样保持不变。最后将光谱调整为无规律状态，只调节 PC-1，从图 5(c)中可以观察到，光谱形状没有改变。因此改变入射光的偏振态不会改变光谱的形状，即证明了双 Sagnac 环滤波器具有偏振无关特性。上述测量结果证明了双 Sagnac 环滤波器的偏振无关和通道间隔的可调特性，这与仿真分析所得出的结论一致。

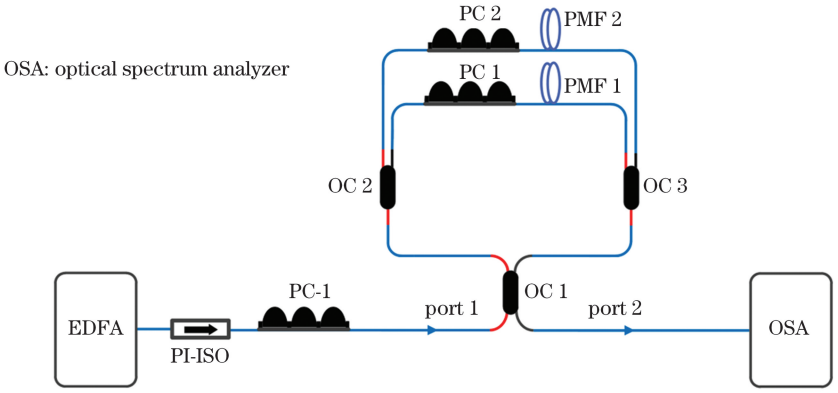

图 3　双 Sagnac 环滤波器传输谱测量的结构图

Fig. 3　Structure diagram for measuring transmission spectrum of double Sagnac loop filter

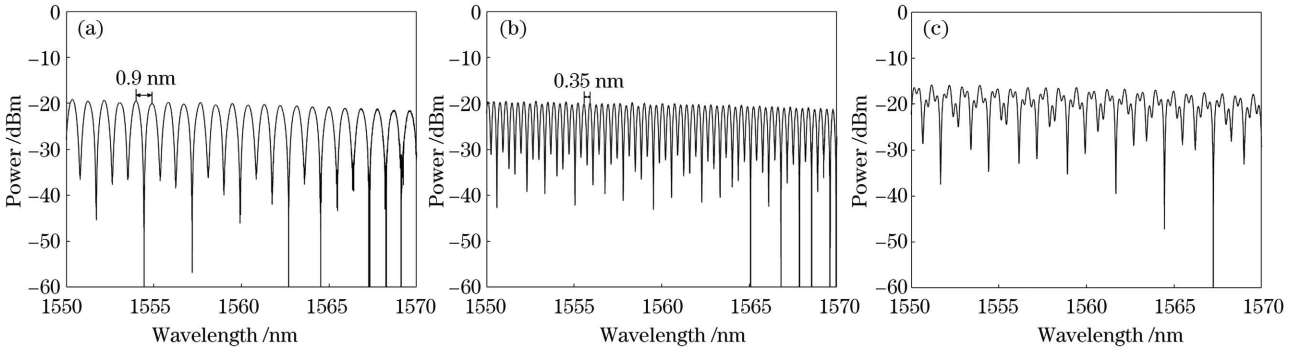

图 4　不同通道间隔下双 Sagnac 环滤波器的透射光谱。(a) 0.9 nm；(b) 0.35 nm；(c)通道间隔无规律

Fig. 4　Transmission spectra of double Sagnac loop filter under different channel spacings. (a) 0.9 nm; (b) 0.35 nm; (c) irregular channel spacing

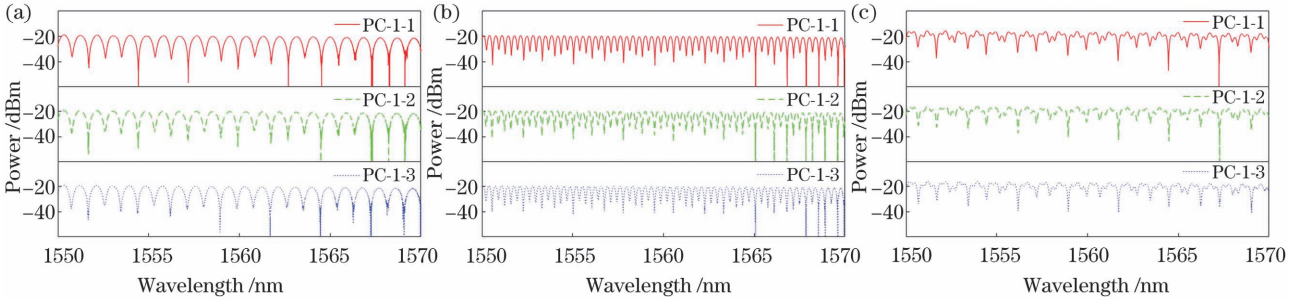

图 5　不同条件下双 Sagnac 环滤波器的透射光谱。(a)通道间隔为 0.9 nm，不同 PC-1 偏转角度；(b)通道间隔为 0.35 nm，不同 PC-1 偏转角度；(c) 通道间隔无规律，不同 PC-1 偏转角度

Fig. 5　Transmission spectra of double Sagnac loop filter under different conditions. (a) Different rotation angles of PC-1 with channel spacing of 0.9 nm; (b) different rotation angles of PC-1 with channel spacing of 0.35 nm; (c) different rotation angles of PC-1 with irregular channel spacing

3.2 基于 FWM 效应和双 Sagnac 环滤波器的通道间隔可调多波长掺铒光纤激光器

本文所设计的基于 FWM 效应和双 Sagnac 环滤波器的通道间隔可调多波长光纤激光器如图 6 所示。一台 980 nm 的泵浦光源提供激励，泵浦光经过 980 nm/1550 nm 的波分复用器（Wavelength Division Multipler，WDM），进入到 5 m 的掺铒光纤（Erbium Doped Fiber，EDF）中进行放大，产生自发辐射光。PI-ISO 用来保证激光在谐振腔中单向振荡。双 Sagnac 环滤波器用来产生多波长激光输出。高非线性光纤（Highly Nonlinear Fiber，HNLF）用于产生 FWM 效应以抑制 EDF 在室温下的均匀展宽[16-18]。OC 4 的 10% 端口作为激光器的输出，由 OSA 进行测量，90% 端口的光流入腔内继续循环。

在本实验中，设置泵浦功率为 512 mW，通过调节双 Sagnac 环滤波器中的 PC 1 和 PC 2，可以实现输出光谱通道间隔的调控，结果如图 7 所示。图 7(a)显示的是通道间隔为 0.9 nm 的多波长输出，对应于仿真光谱中的图 2(a)和测量结果中的图 4(a)。图 7(b)显示的是通道间隔为 0.35 nm 的多波长输出，对应于仿真光谱中的图 2(b)和测量结果中的图 4(b)。在整个过程中，通道间隔的切换不仅是可逆的，而且可重复性良好。值得注意的是，图 7(a)显示输出波长的间隔不是严格等于 0.9 nm，图 7(b)显示输出波长的间隔也不是严格等于 0.35 nm，这是因为光谱烧孔（Spectral Hole Burning，SHB）效应影响了光谱的波长间隔[13,19]。此外，由于双 Sagnac 环滤波器是偏振无关器件，在与其他偏振相关的滤波器或者偏振相关的模式竞争抑制器件进行组合时，能有效地避免激光器系统中光学器件偏振互扰的问题[20-21]。

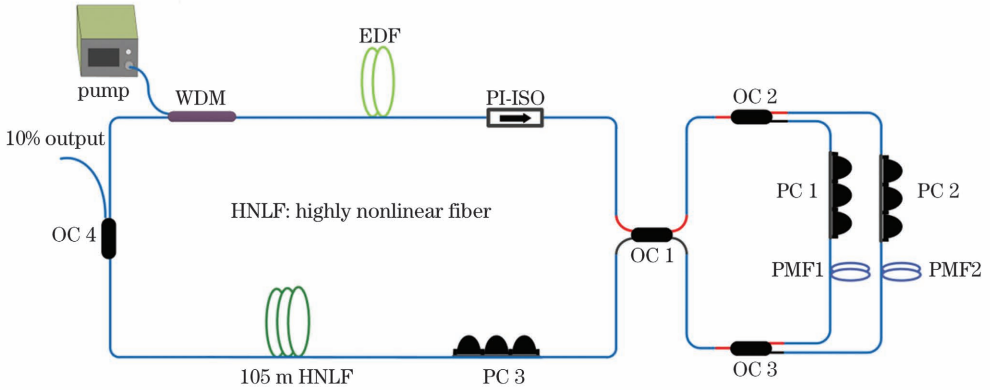

图 6　基于 FWM 效应和双 Sagnac 环滤波器的通道间隔可调多波长掺铒光纤激光器的实验装置

Fig. 6　Experimental setup of channel spacing tunable multi-wavelength erbium-doped fiber laser utilizing double Sagnac loop filter and FWM effect

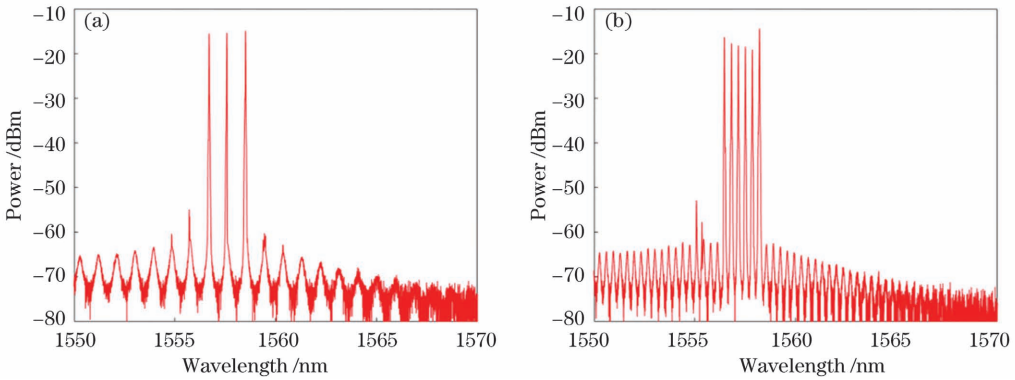

图 7　多波长输出的光谱。(a)通道间隔为 0.9 nm；(b)通道间隔为 0.35 nm

Fig. 7　Multi-wavelength output spectra. (a) Channel spacing of 0.9 nm; (b) channel spacing of 0.35 nm

4　结　　论

对一种由两段不同长度 PMF 并联构成的双 Sagnac 环滤波器的传输特性进行了详细的理论分析、仿真实验以及实验测量，证明了滤波器的偏振无关和通道间隔可调特性。根据仿真结果和测量结果，设计了一种基于 FWM 效应和双 Sagnac 环滤波器的通道间隔可调多波长掺铒光纤激光器，该激光

器可以实现 0.35 nm 和 0.9 nm 两种通道间隔的多波长输出。由于双 Sagnac 环滤波器具有偏振无关特性，偏振相关的器件结构并不会与滤波器发生偏振互扰。双 Sagnac 环滤波器结构简单，具有偏振无关和通道间隔可调的良好特性，在多波长光纤激光器中会有很大的应用潜力。

参 考 文 献

[1] Zhou X F, Zhou Y, Li Z Y, et al. Research on temperature sensing characteristics with cascaded fiber Sagnac interferometer and fiber Fabry-Perot interferometer-based fiber laser [J]. Optical Engineering, 2019, 58(5): 057103.

[2] Fang S S, Wu X Q, Zhang G, et al. High-sensitivity fiber optic temperature and strain sensors based on the vernier effect [J]. Chinese Journal of Lasers, 2021, 48(1): 0106004.
方莎莎, 吴许强, 张刚, 等. 基于游标效应的高灵敏光纤温度和应变传感器[J]. 中国激光, 2021, 48(1): 0106004.

[3] Zhang F L, Zhai S, Pan J, et al. Three-dimensional multi-microring resonance filter based on Sagnac-like interferometer[J]. Chinese Journal of Lasers, 2020, 47(11): 1113003.
张福领, 翟珊, 潘俊, 等. 类 Sagnac 干涉仪结构的三维多微环谐振滤波器[J]. 中国激光, 2020, 47(11): 1113003.

[4] González-García A, Pottiez O, Grajales-Coutiño R, et al. Switchable and tuneable multi-wavelength Er-doped fibre ring laser using Sagnac filters[J]. Laser Physics, 2010, 20(3): 720-725.

[5] Kim R K, Han Y G. Switchable multiple lasing oscillations in an erbium-doped fiber ring laser using a single stage of a Sagnac loop mirror [J]. Applied Physics B, 2011, 103(4): 813-818.

[6] Chen D R. Stable multi-wavelength erbium-doped fiber laser based on a photonic crystal fiber Sagnac loop filter[J]. Laser Physics Letters, 2007, 4(6): 437-439.

[7] Wang H P, Wang L, Shi G H, et al. Stable multi-wavelength fiber laser with single-mode fiber in a Sagnac loop [J]. Applied Optics, 2016, 55(12): 3339-3342.

[8] Cheng J Q, Chen W C, Chen G J. Switchable quadruple-wavelength Erbium-doped fiber laser based on a chirped fiber grating and polarization-maintaining fiber[J]. Optics & Laser Technology, 2016, 78: 71-73.

[9] Li F, Feng X H, Zheng H, et al. Multiwavelength lasers with homogeneous gain and intensity-dependent loss[J]. Optics Communications, 2011, 284(9): 2327-2336.

[10] He Z X, Zhang P, Wu D, et al. 1.7 μm tunable multi-wavelength Raman fiber laser based on amplified spontaneous emission pump[J]. Laser & Optoelectronics Progress, 2020, 57(7): 071403.
贺振兴, 张鹏, 吴迪, 等. 基于 ASE 泵浦的 1.7 μm 波段可调谐多波长拉曼光纤激光器实验研究[J]. 激光与光电子学进展, 2020, 57(7): 071403.

[11] He W, Shangguan C M, Zhu L Q, et al. Tunable and stable multi-wavelength erbium-doped fiber laser based on a double Sagnac comb filter with polarization-maintaining fibers [J]. Optik, 2017, 137: 254-261.

[12] Zhu K, Pei L, Zhao Q, et al. Switchable multi-wavelength fiber laser utilizing double Sagnac loop filter[J]. Infrared and Laser Engineering, 2020, 49(11): 20200047.
朱可, 裴丽, 赵琦, 等. 采用双 Sagnac 环滤波器的可切换多波长光纤激光器[J]. 红外与激光工程, 2020, 49(11): 20200047.

[13] Tang M, Jiang Y C, Li H S, et al. Multi-wavelength fiber laser based on dual-Sagnac comb filter for LP11 modes output[J]. Journal of Lightwave Technology, 2020, 38(14): 3745-3750.

[14] Zhao Q, Pei L, Wang J S, et al. Interval-adjustable multi-wavelength erbium-doped fiber laser with the assistance of NOLM or NALM[J]. IEEE Access, 2021, 9: 16316-16322.

[15] Zhao Q, Pei L, Zheng J J, et al. Tunable and interval-adjustable multi-wavelength erbium-doped fiber laser based on cascaded filters with the assistance of NPR[J]. Optics & Laser Technology, 2020, 131: 106387.

[16] Wang P H, Weng D M, Li K, et al. Multi-wavelength erbium-doped fiber laser based on four-wave-mixing effect in single mode fiber and high nonlinear fiber[J]. Optics Express, 2013, 21(10): 12570-12578.

[17] Ahmad H, Ahmed M H M, Samion M Z, et al. All fiber multiwavelength Tm-doped double-clad fiber laser assisted by four-wave mixing in highly nonlinear fiber and Sagnac loop mirror [J]. Optics Communications, 2020, 456: 124589.

[18] Zhao Q, Pei L, Tang M, et al. Switchable multi-wavelength erbium-doped fiber laser based on core-offset structure and four-wave-mixing effect [J]. Optical Fiber Technology, 2020, 54: 102111.

[19] Feng S C, Xu O, Lu S H, et al. Switchable multi-wavelength erbium-doped fiber lasers based on a Mach-Zehnder interferometer using a twin-core fiber

[J]. Chinese Physics Letters, 2009, 26(6): 064208.

[20] Zhang X. Study on fiber laser and fiber sensor based on tunable Sagnac loop[D]. Harbin: Harbin Institute of Technology, 2016: 31-32.
张新. 基于可调谐 Sagnac 环的光纤激光器和光纤传感器的研究[D]. 哈尔滨: 哈尔滨工业大学, 2016: 31-32.

[21] Liu X S, Zhan L, Luo S Y, et al. Individually switchable and widely tunable multiwavelength erbium-doped fiber laser based on cascaded mismatching long-period fiber gratings[J]. Journal of Lightwave Technology, 2011, 29(21): 3319-3326.

Analysis and Experimental Study on Transmission Characteristics of Double Sagnac Loop Filter

Cui Wenxiang[1], Zhou Xuefang[1*], Hu Miao[1], Bi Meihua[1], Yang Guowei[1], Li Qiliang[1], Wang Tianshu[2]

[1] *School of Communication Engineering, Hangzhou Dianzi University, Hangzhou, Zhejiang* 310018, *China*;
[2] *Institute of Space Optoelectronics Technology, Changchun University of Science and Technology, Changchun, Jilin* 130022, *China*

Abstract

Objective An optical fiber Sagnac loop has been widely used to manufacture optical fiber sensors and optical fiber Sagnac loop filters because of its excellent characteristics such as simple structure, low insertion loss, and low cost. However, the single Sagnac comb filter cannot meet the requirements of some practical laser systems due to its fixed channel spacing. Recently, some research groups have proposed multi-wavelength erbium-doped fiber lasers based on a double Sagnac loop filter, however the transmission characteristics of this filter have not been investigated, which restricts its application in the fields of multi-wavelength fiber lasers and optical fiber sensing. Therefore, in this study, the transmission characteristics of a double Sagnac loop filter constructed by two segments of polarization-maintaining fiber (PMF) in parallel are analyzed and discussed. The measurement results of transmission characteristics are consistent with those obtained by theoretical analysis. Moreover, a channel-spacing tunable multi-wavelength erbium-doped fiber laser utilizing a double Sagnac loop filter with the assistance of four wave mixing (FWM) effect is experimentally demonstrated. Therefore, it is significantly important to analyze and experimentally investigate the transmission characteristics of a double Sagnac loop filter, which is helpful for the design of future multi-wavelength fiber lasers.

Methods In this study, the transmission function of a double Sagnac loop filter is first calculated in detail by the transmission matrix theory, and the incident light is assumed to be in an arbitrary polarization state. Then, the simulated transmission spectra are carried out by the Matlab software. The theoretical analysis and simulation results indicate that the double Sagnac loop filter has the polarization-independent characteristic and the tunable channel spacing. To demonstrate the transmission characteristics of the double Sagnac loop filter, the experimental apparatus for measuring the transmission spectra of the filter is designed. Note that we insert a polarization controller (PC) between the erbium-doped fiber amplifier and the double Sagnac loop filter to control the polarization state of the light entering into the filter. Finally, in order to verify the tunable channel spacing of the double Sagnac loop filter in the laser system, we implement the double Sagnac loop filter in the erbium-doped fiber laser while using a highly nonlinear fiber to provide the FWM effect.

Results and Discussions The transmission function of a double Sagnac loop filter is obtained by adopting the transmission matrix theory. Based on the results of theoretical analysis, the transmission spectra of the double Sagnac loop filter are simulated. In this study, the lengths of PMF 1 and PMF 2 are 6.6 m and 13.51 m, respectively. The birefringence differences of PMF 1 and PMF 2 are 4.0×10^{-4} and 5.1×10^{-4}, respectively. When the polarization angle of PC 1 (θ_1) is $\pi/6$ and the polarization angle of PC 2 (θ_2) is 0, the channel spacing of the filter is 0.9 nm [Fig. 2(a)]. When $\theta_1=0$ and $\theta_2=\pi/6$, the channel spacing of the filter is 0.35 nm [Fig. 2(b)]. In the transmission characteristic test of the double Sagnac loop filter, by adjusting PC 1 and PC 2, the measured

transmission spectra with channel spacings of 0.9 nm and 0.35 nm are obtained [Figs. 4(a) and 4(b)], which are consistent with the simulation results [Figs. 2(a) and 2(b)]. Furthermore, a irregular spectrum [Fig. 4(c)], corresponding to the situation that $\theta_1 \neq 0$ and $\theta_2 \neq 0$ in Eq. (11), can be observed by appropriately tuning the orientations of PC 1 and PC 2. When the channel spacing of the spectrum is fixed (0.35 nm, 0.9 nm, or irregular channel spacing), the spectral shape remains unchanged (Fig. 5) in spite of arbitrarily adjustment of the polarization angle of PC-1. Therefore, adjusting the polarization state of the incident light cannot influence the transmission spectra of the double Sagnac loop filter, indicating that it is a polarization-independent filter. Based on the theoretical analysis and measurement results of the double Sagnac loop filter, a channel spacing tunable multi-wavelength fiber laser utilizing a double Sagnac loop filter with the assistance of the FWM effect is proposed. A highly nonlinear fiber with a length of 105 m is used to effectively alleviate the mode competition. When the pump power is set to be 512 mW, the triple-wavelength lasing with a channel spacing of 0.9 nm [Fig. 7(a)] and a sextuple-wavelength lasing with a channel spacing of 0.35 nm [Fig. 7(b)] can be achieved by tuning PC 1 and PC 2, which are accordance with the simulation results [Figs. 2(a) and 2(b)] and measurement results [Figs. 4(a) and 4(b)]. It is worth noting that the channel spacing tuning process is reversible and has good repeatability.

Conclusions In this study, the transmission characteristics of a double Sagnac loop filter, composed of two segments of PMF in parallel, are analyzed, simulated and measured in detail, which proves that the proposed double Sagnac loop filter has the polarization-independent characteristic and the tunable channel spacing. According to the results of simulation and measurement, a channel spacing tunable multi-wavelength erbium-doped fiber laser utilizing a double Sagnac loop filter with the assistance of the FWM effect is designed. The laser can output multi-wavelength lasing lines with channel spacings of 0.35 nm and 0.9 nm. Owing to the polarization-independent characteristic of the double Sagnac loop filter, the polarization-dependent devices are not interfere with the transmission spectra of the filter. Thus, the double Sagnac loop filter exhibits the simple structure, polarization-independence, the tunability of channel spacing, and a great potential application in the field of multi-wavelength fiber lasers.

Key words fiber optics; optical filter; transmission matrix theory; double Sagnac loop; channel spacing tunability; polarization independence